Korean J. Chem. Eng., 40(6), 1540-1547 (2023)
DOI: 10.1007/s11814-023-1393-3

pISSN: 0256-1115
eISSN: 1975-7220

Excellent physical durability and enhanced Fano absorption of SPR sensor platform based on Au-covered silica sphere monolayer

Baeck Choi*,,***,†, Dae Keun Park**, Sin-Yen Leo*, and Peng Jiang***

*Department of Chemical Engineering, University of Florida, Gainesville FL 32611, USA
**Energy and Environment Laboratory, Korea Electric Power Corp. Research Institute, Daejeon 34056, Korea
***New Energy Technologies Laboratory, Korea Electric Power Corp. Research Institute, Naju 58277, Korea
(*Received 22 November 2022 • Revised 19 December 2022 • Accepted 31 December 2022*)

Abstract−It is essential to secure the optical performance (sensitivity, FOM, plasmonic absorption strength, etc.), large-area fabrication, and physical durability to improve the usability of nanostructured SPR sensors. In this study, to ensure the physical durability of an Au-covered silica sphere monolayer (Au film over nanosphere (AuFON)) manufactured for use as an SPR sensor platform, the sensing performance and physical durability after TMOS treatment to bind spherical silica particles were investigated. The peel-off test showed that Au and silica constituting the AuFON did not fall off, and there was no significant difference in the sensing sensitivity and plasmonic absorption intensity before and after TMOS treatment. In addition, when colloidal Au nanoparticles (diameter of 5 nm) were applied to as-prepared AuFON and heat-treated, it was confirmed that the Au shells of the plasmonic particles were interconnected, and the Fano intensity increased from 3-5% to 22%.

Keywords: Surface Plasmon Resonance (SPR), Colloidal Self-assembly, Fano Resonance, TMOS, Colloidal Au Nanoparticles, AuFON

INTRODUCTION

In fields such as manufacturing, agriculture, environment, transportation, and medical care, the successive collection of data and further utilization using the Internet of Things (IoT), artificial intelligence (AI), and big data is becoming more critical. If a biosensor with excellent sensitivity and selectivity is used, effective direct sensing is possible without an additional pre-treatment of the patient sample [1,2]. In addition, if continuous data can be effectively obtained to evaluate the short- and long-term process capability of a unit process such as Cpk or Z value in the manufacturing industry, the risk to consumers and the cost burden to producers can be significantly reduced [3]. In the hydrogen production process, low concentrations of hydrogen can cause serious safety accidents, such as fires and explosions. Therefore, quickly and accurately sensing the hydrogen concentration helps realize a safer hydrogen economy [4-8]. Anyway, to secure the usability of the nanostructure-based sensor that can be applied to various industries, sensing performance and durability [9-13] still need to be improved. In particular, the excellent durability of the nanostructured sensor platform makes it possible to use it in the actual measuring environment [14]. Attempts to secure the durability of metal components via surface reconstruction by heat treatment or electrochemical reconstruction have been found [15,16]. Another example is to cover the plasmonic particle with a metal oxide or polymer [17,18]. However, finding the result of preventing damage to the SPR sensor platform from the external force is not easy.

A surface plasmon resonance (SPR) sensor is a direct sensing technique that does not require chemical labeling and is particularly attracting attention for its application to bio and gas sensors [19-21]. SPR dips appear as the minimum or maximum of a specific optical spectrum when plasmon waves are excited by an external light source. Therefore, the efforts to prepare the nanostructured SPR sensor platform with top-down or bottom-up approaches continue to replace bulky and complex prism-based SPR sensor systems [9,22-25]. In particular, a scalable and low-cost bottom-up approach enables fine structure control of both metals and dielectrics, significantly improving the sensitivity (S, nm/RIU) and figure of merit (FOM, Sensitivity/FWHM) [22-24]. The bottom-up approach, which does not require an expensive patterned mold, also has economic advantages. Previously, we reported on the fabrication of an Au-covered silica sphere monolayer (Au film over nanosphere (AuFON)) using the colloidal Langmuir-Blodgett process and SPR sensing sensitivity [29]. As a result, it was confirmed that the sensing sensitivity increased as the diameter of the silica sphere particles increased from 200 to 400, 700, and 1,000 nm, and the plasmon mode decreased from high-order to Fano resonance (FR) and dipole mode. Indeed there are already many studies on plasmonic particles composed of a dielectric core and a metal shell [30-37]. In our case, plasmonic particle arrays were manufactured using silica sphere particles with various diameters. As a result, the trend of SPR sensing sensitivity according to the diameters and plasmon mode was confirmed. However, the problems still to be solved are the poor physical durability of the AuFONs and the low plasmonic absorption intensity of the FR mode. If the nanostructured SPR sensor platform is easily damaged, even by a weak external force

†To whom correspondence should be addressed.
E-mail: baeckchoi@gmail.com, b.choi@kepco.co.kr

sufficient to sweep it with a fingertip, it will be challenging to use in practice.

In general, FOM is used to express the accuracy of SPR sensing. FOM can be obtained by dividing the sensitivity by the FWHM of the SPR dip waveform [26-28]. In this simple calculation, consideration of the SPR dip intensity is insufficient. When the SPR dip intensity is sufficiently large and the FWHM is small, plasmon resonance can be observed more accurately. The linear characteristic of Fano resonance is caused by interference between the plasmonic modes of the plasmonic particles [9,38-41]. Fano absorption is generally not observed for a single particle. However, when plasmonic particles form oligomers (e.g., dimers, trimers, tetramers, and arrays), narrow, deep, and sometimes asymmetrical line shapes are observed. Fano resonance is receiving wide attention in SPR sensing because such a sharp and asymmetrical SPR dip effectively identifies the resonance. In addition, it has been reported that modulation of the Fano resonance is possible owing to various methods, such as asymmetry or broken harmony in the arrangement of plasmonic particles [42,43]. It controls the distance between plasmonic particles or arranges the particles of different structures (shape, size, aspect ratio, etc.) to utilize interference or overlap between plasmon modes [44-46]. However, if it can be obtained only through complicated semiconductor manufacturing processes, such as photolithography and precise positioning of plasmonic particles using AFM tips, it is challenging to obtain economic benefits in manufacturing the SPR sensor platform [30]. The fabrication of a silica sphere monolayer using the colloidal Langmuir-Blodgett coating process and further Au sputter deposition was effective in fabricating a large-area SPR sensor platform. However, it is recommended the SPR sensing accuracy by increasing the Fano intensity.

In this study, we introduce a simple and effective method to obtain the physical durability of AuFONs and enhance the intensity of the Fano resonance. Silica spherical particles of AuFON were bonded together by further hydrolysis and condensation with tetramethoxysilane (TMOS). In addition, colloidal Au nanoparticles were applied to the as-prepared AuFON and annealed to bond the hemispherically coated Au layer. Consequently, the changes in the physical and optical properties of AuFONs according to these attempts were investigated with optical experiments and further FDTD simulations.

EXPERIMENTAL

1. Langmuir-Blodgett Coating and Au Sputter Deposition

The as-prepared silica spherical particles (1,000 nm in diameter) were washed with ethanol (200 Proof, Decon Labs) six times. It was composed of sequential centrifugation (4,000 rpm for 30 min) and re-dispersion in ethanol. It was then dispersed in ethylene glycol (Sigma-Aldrich) at a volume fraction of 2.0%. A glass slide (plain microscope glass slides (25×75×1.0 mm, Fisher Scientific) was placed into a 1.0% ammonium persulfate (APS, Sigma-Aldrich) solution in ethanol for 2 h. The dispersion of silica spherical particles in ethylene glycol was then added dropwise to the Millipore water (18.2 mΩ) surface filled in the bath. A vertically immersed glass in the water bath was forcibly moved up with 12.5 mm per min of running speed controlled by a syringe pump (KDScientific780-230). It was then oven dried at 80 °C for 3 h. The as-prepared LB films of the silica sphere particle array were finally Au-coated (coating thickness of 50 nm) by sputter deposition using Kurt J. Lesker CMS-18 Multi-Target Sputter (Nanoscale Research Facility (NRF), University of Florida).

2. Additional Treatment of AuFON with TMOS or Colloidal Au Nanoparticles

The TMOS treatment for additional silica formation on the AuFON was as follows. Two bottles and the as-prepared AuFON were placed inside a sealed plastic container. The first bottle contained tetramethyl orthosilicate (99%, Sigma-Aldrich), and the second contained Millipore water. The sealed container was maintained at 80 °C for 2, 4, and 8 h and then dried. Next, colloidal Au nanoparticles in toluene (0.01 g/ml, dodecanethiol-functionalized Au nanoparticles with 5 nm of diameter, Nanoprobes) were spread on an as-prepared AuFON with a spray gun (Iwata). Subsequently, it was heat-treated at 300 °C for 8 h in air.

3. Photo/SEM Images and Peel-off Test

Images were captured using a digital camera (EOS Rebel T5, Canon). Scanning electron microscopy (SEM) images were obtained using an electron microscope (JEOL CarryScope 5700, Nanoscale Research Facility (NRF) at the University of Florida) without further metal deposition. Finally, the peel-off test was performed by attaching a plastic tape firmly and peeling it.

4. Normal-Incidence Reflection Spectra and Finite Difference Time Domain (FDTD) Simulation

SPR properties were investigated by measuring normal-incidence specular optical reflection spectra using high-resolution Vis-NIR (HR4000, Ocean Optics) and NIR (NIR-512, Ocean Optics) spectrometers. A tungsten halogen lamp (LS-1, Ocean Optics) and a halogen lamp (DH-2000, Mikropack) were used as light sources. The solvents were placed on the surface of AuFON, and reflection spectra were measured sequentially. Methanol, acetone, ethanol, isopropyl alcohol (IPA), butanol, tetrahydrofuran (THF), dichloromethane, and toluene were used for the refractive index. An FDTD simulation (FDTD Solutions 8.60, Lumerical Solutions) was performed to solve the Maxwell equation to obtain the electric field distribution and simulated reflection spectra. Simulation models were established using an HCP silica sphere particle array on a rectangular glass substrate. Then, the Au ellipsoid particles were placed on the silica sphere particles and were designated to have a coating thickness of 50 nm. The override mesh order was set to ensure that the Au hemisphere covered the silica nanosphere particle structure. Before the simulation, the refractive index was monitored in the z-direction. In addition, mode expansion was set up in the x-, y-, and z-directions to monitor the electric field distribution.

RESULTS AND DISCUSSION

1. Physical Stability of AuFON with TMOS Treatment

The SPR sensing sensitivity of AuFON prepared by Au sputter deposition on a silica sphere monolayer on a glass surface has been reported previously [26]. Spherical silica particles with a diameter of 200, 400, 700, and 1,000 nm were formed using the colloidal Langmuir-Blodgett coating process. In addition, it was confirmed that the larger the silica sphere diameter (1,000>700>400>200 nm)

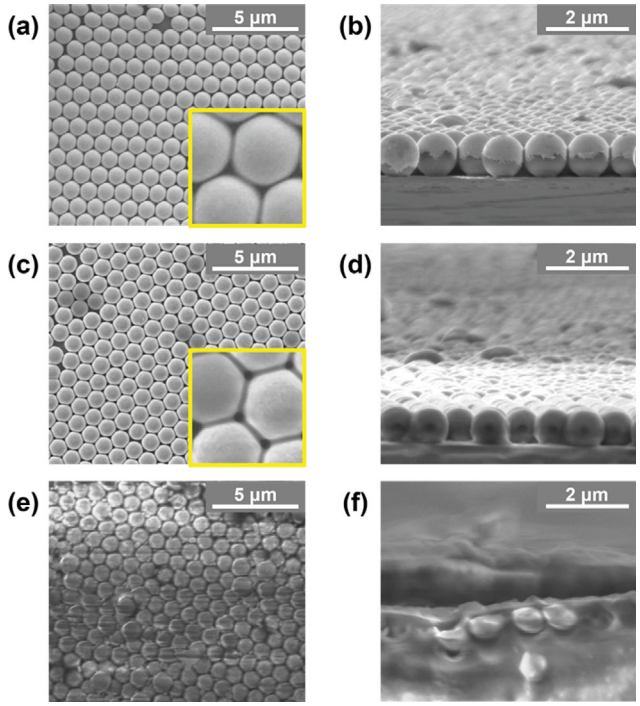

Fig. 1. (a) Top and (b) cross-sectional SEM images of the as-prepared AuFON. (c) Top and (d) cross-sectional SEM images of AuFON after 2 h of TMOS treatment. (e) Top and (f) cross-sectional SEM images of AuFON after 8 h of TMOS treatment.

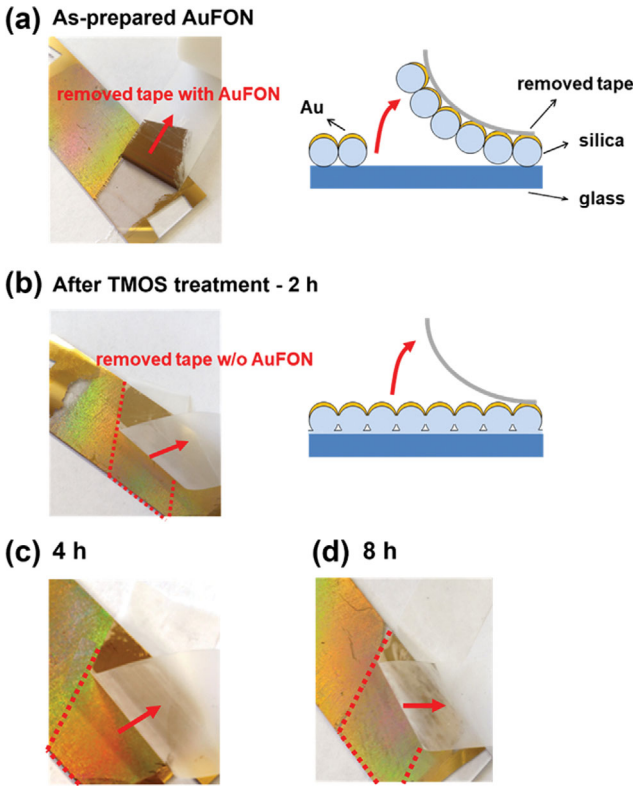

Fig. 2. Photo and illustration after the peel-off test of (a) as-prepared AuFON and AuFON after (b) 2, (c) 4, and (d) 8 h of TMOS treatment.

and the lower the plasmon mode (dipole>high order), the higher the sensitivity. However, through these studies, it was recognized that it is also practically essential to ensure the physical durability of the SPR sensor platform. An as-prepared AuFON is easily damaged even with a weak force swept with the fingertips. The solvents with different refractive indices were placed on the top surface of the nanostructured SPR sensor platform to examine the sensitivity experimentally. The positions of the light source and probe on the surface of the SPR sensor platform were precisely fixed, the solvent was placed, and the normal-incidence reflection spectrum was measured. However, an SPR sensor platform was also easily damaged while replacing the solvent.

Silica can be manufactured using various methods, and the dry approach is known to have advantages in particle size, distribution, and purity control because of its feasible reaction control. Silicon tetrachloride ($SiCl_4$), tetraethyl orthosilicate (TEOS), and tetramethyl orthosilicate (TMOS) are used to manufacture silica. When a metal alkoxide is used as a precursor, it can be prepared through a sol-gel method that undergoes hydrolysis, alcohol condensation, and water condensation. This process was applied to as-prepared AuFON at 80 °C in a sealed container. Fig. 1(a), (b) shows the top and cross-sectional SEM images of the as-prepared AuFON with a diameter of 1,000 nm. It can be seen that a hexagonal close-packed (HCP) structure is formed uniformly. Fig. 1(b) clearly shows the hemisphere-coated Au layer. Fig. 1(c), (d) shows AuFON after 2 h of TMOS treatment.

The inset image in Fig. 1(c) shows that the plasmonic particles are bound to each other, compared to Fig. 1(a). Fig. 1(d) shows the connection between the plasmonic particles and the glass substrate. Fig. 1(e), (f) shows the structure after 8 h of TMOS treatment, which is observed to be crushed. It was challenging to focus the electron beam during the SEM measurement. Therefore, a blurry image was obtained, because silica, a dielectric, was excessively formed on the AuFON surface. Fig. 2 shows a photograph and illustration after attaching and removing the plastic tape to the AuFON. As prepared AuFON, it was observed that the formed Au and silica sphere monolayer fell off cleanly. In the case of AuFON treated with TMOS, no detachment was observed (Fig. 2(b), (c), (d)). The dotted line in Fig. 2 shows the location where the plastic tape was attached. The Au or silica attached to the removed plastic tape is not visible. Even without sophisticated test equipment to evaluate peel adhesion, an apparent result could be obtained by attaching and peeling the plastic tape on the AuFON platform. Adhesion testing equipment was also utilized to measure the adhesive strength value, but adhesion strength over time of the TMOS treatment could not be obtained. It is because there was no detachment after TMOS treatment. As a result, the bonding between silica sphere particles and between silica and glass substrate by additional TMOS treatment contributed significantly to the improvement of the physical durability of AuFON.

The line shape in the measured normal-incidence reflection spectra in Fig. 3(a) did not differ significantly before and after TMOS treatment. However, despite no significant change in the wave-

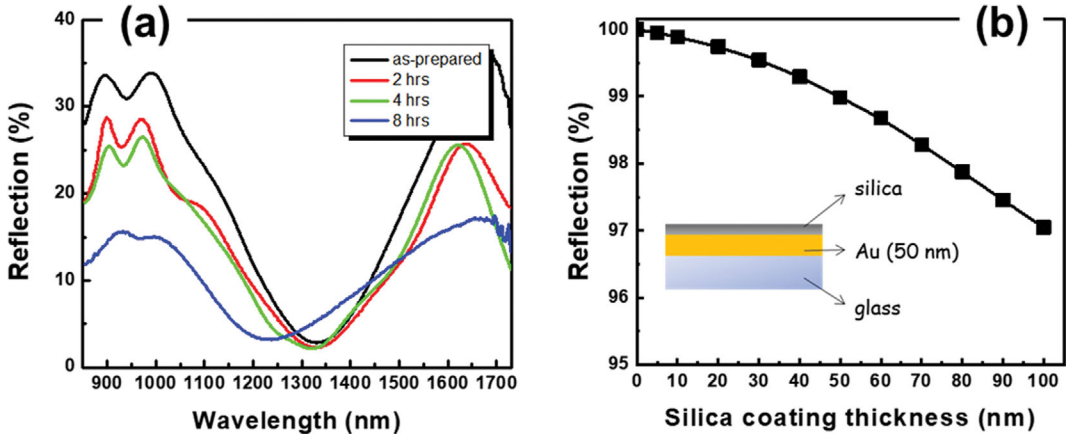

Fig. 3. (a) Experimentally measured normal-incidence reflection spectra of AuFON before and after the TMOS treatment. (b) Calculated reflectance of incident light with a wavelength of 900 nm according to the silica layer thickness on the Au surface and Fresnel equation.

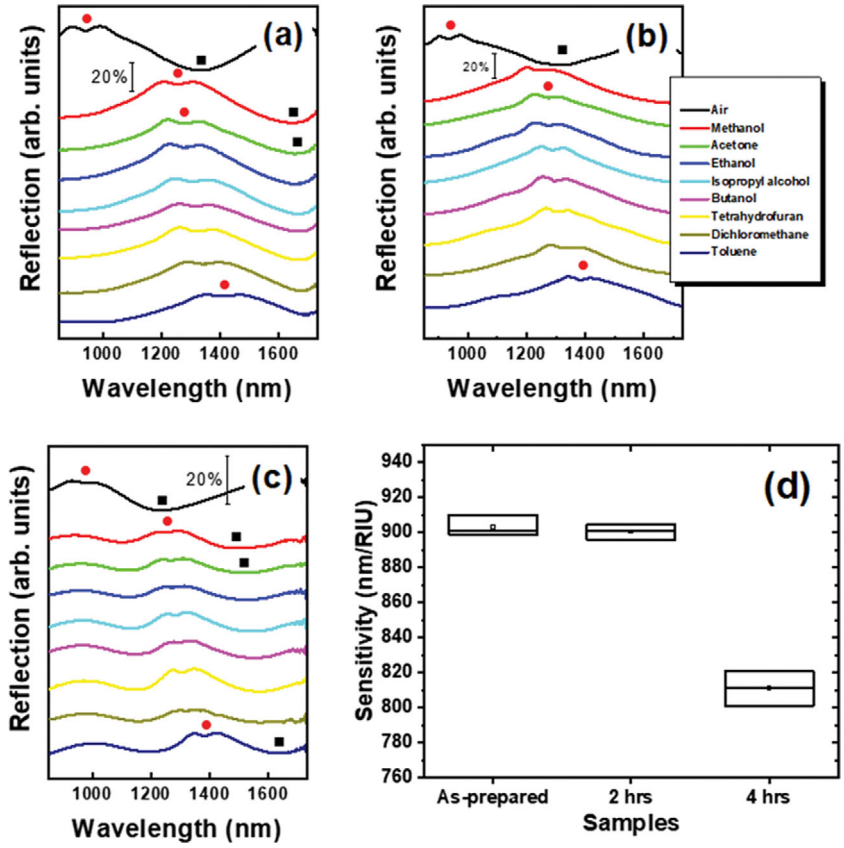

Fig. 4. Experimental sensing tests for (a) as-prepared AuFON. Those for AuFON for (b) 2 h and (c) 4 h of TMOS treatment. (d) Box plot of SPR sensing sensitivity based on the Fano resonance.

form, the reflection intensity (%) gradually decreased in the near-IR region, especially where Fano absorption appeared. It is because the silica layer additionally formed on the as-prepared AuFON surface acted as an anti-reflection coating, which can be easily predicted using the Fresnel equation. If the reflection at a wavelength of 900 nm is calculated according to the thickness of the silica formed on the Au surface using the Fresnel equation, it can be seen in Fig. 3(b). A decrease in the reflection intensity of about 3% is observed with the silica thickness of 100 nm. However, after 8 h of TMOS treatment, the reflection intensity was reduced by up to 10 to 20%. It is because the additional formation of non-uniform silica in the regular embossed structure had to occur. In addition, because the size of the optical probe used to measure the reflection spectrum was approximately 1 mm, it was impossible to measure the reflection spectrum at an exact location.

Fig. 4 shows the results of the sequential reflection spectrum

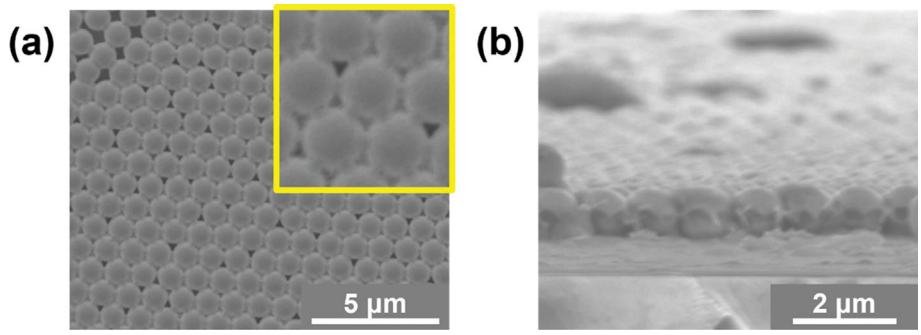

Fig. 5. (a) Top and (b) cross-sectional SEM images of AuFON after treatment with colloidal Au nanoparticles.

measurements with various solvents. These volatile organic solvents were used because replacing them from the AuFON surface is effortless. It was necessary to remove the solvent used to measure the reflection spectrum at the exact location of the SPR sensor platform. As previously reported, the absorption of the dipole mode represented by the black square in Fig. 4 shows the highest sensing sensitivity of approximately 970 nm/RIU. However, because the plasmon absorption strength is high and the width is so broad that it is difficult to specify the broadening of the SPR dip, the accuracy is low.

On the other hand, although the sensitivity of the Fano resonance is approximately 903 nm/RIU, which is slightly lower than that of the dipole mode, it has a narrow and deep waveform, so specifying the SPR dip position is quite feasible. As shown in Fig. 4(d), which summarizes the sensitivity of the Fano resonance according to the additional silica formation time, the AuFON obtained through the addition of silica for 2 h did not differ significantly from that of the as-prepared sample with a sensitivity of 901 nm/RIU. In the case of AuFON treated with TMOS for 4 h, it was observed that not only was the average sensitivity of Fano resonance as low as 810 nm/RIU, but also the box plots showing the upper and lower limits of 75% and 25% are enlarged. The SEM images in Fig. 1(e), (f) and the box plot in Fig. 4(d) show the structural non-uniformity of AuFON caused by excessive TMOS treatment may adversely affect the sensing sensitivity.

2. Effects of Connecting Hemispherically Coated Au Layer Using Colloidal Au Nanoparticles

Porous materials manufactured using templates are diverse, ranging from polymers and ceramics to metals [47-49]. The ordered porous metal structure can be applied to electrochemical sensors, catalytic converters, and fuel cells, so research on manufacturing and application is actively underway [50-53]. By applying chemical reduction or electroplating of the metal precursor together with the template and then removing the template appropriately, porous metals can be prepared. In addition, porous metal structures can be manufactured using colloidal nanoparticles. The interstitial space of the template is filled with colloidal nanoparticles, heat treatment is completed, and the template is removed [49].

These colloidal Au nanoparticles are widely used to form a porous metal structure (e.g., inverse opal structure), while well-ordered 2D or 3D colloidal particles are used as a structural template [54,55]. The colloidal Au nanoparticles are prepared by so-called 'bi-phase (or two phases) liquid-liquid reduction' for thiol-functionalized Au nanoparticles in 3-5 nm of particle diameter [56]. In this method, a dissolved Au precursor (hydrogen tetrachloroaurate (H_2AuCl_4)) in water and tetraoctylammonium bromide (TOAB) in toluene were mixed vigorously, and the phase of the Au precursor was transferred from water to toluene. The Au precursor ($AuCl_4^-$) in toluene was reduced by sodium borohydride ($NaBH_4$) in the presence of dodecanethiol. Then dodecanethiol-functionalized colloidal Au nanoparticles were formed successively. Colloidal Au nanoparticles were coated on the surface of the as-prepared AuFON by spray coating, and the structure and optical characteristics were examined after heat treatment at 300 °C for 8 h. Fig. 5(a), (b) shows the top- and cross-sectional SEM images of colloidal Au nanoparticle-treated AuFON (1,000 nm of silica sphere diameter). At first glance, it was observed that Au coated with hemispheres on the surface of silica particles were bound to each other in a bridge structure with excellent uniformity. Fig. 5(b), the cross-sectional SEM image, shows that the silica surface was not fully covered with Au. The silica was exposed at the bottom of the plasmonic particles without coating with the Au layer. Fig. 6(a) shows experimentally measured normal-incidence optical reflection spectra. After treatment with colloidal Au nanoparticles, the reflection intensity (%) increased by 20-50% over the entire NIR region. The increase in the reflection intensity may result from the area not entirely deposited by sputter deposition being filled by treatment with colloidal Au nanoparticles or the increase in the thickness of the Au hemisphere coating. As with AuFON, plasmon absorption due to dipole and Fano resonance was observed in NIR. After treatment with colloidal Au nanoparticles, the dipole dip position changed from 1,330 to 1,182 nm. In the case of Fano absorption, the position shift was from 940 to 958 nm, while its intensity was approximately 22%, and that of the as-prepared AuFON was only 3-5%. This increased Fano intensity can indicate resonance in the sensing tests. Resonance spectra in the sensing tests where various organic solvents are used as a reference for the refractive index appear more evident than the results of as-prepared AuFON in Figs. 6(b) and 4(a). The SPR sensing sensitivities for dipole and Fano resonance were 1,035 and 883 nm/RIU, as shown in Fig. 6(c).

The average full width half maximum (FWHM) of the Fano absorption is approximately 59.31±5.30, so the figure of merit (FOM) is ~15. This number is lower than the as-prepared AuFON (~21 of FOM with 42.99±3.04 of FWHM), but highly increased Fano

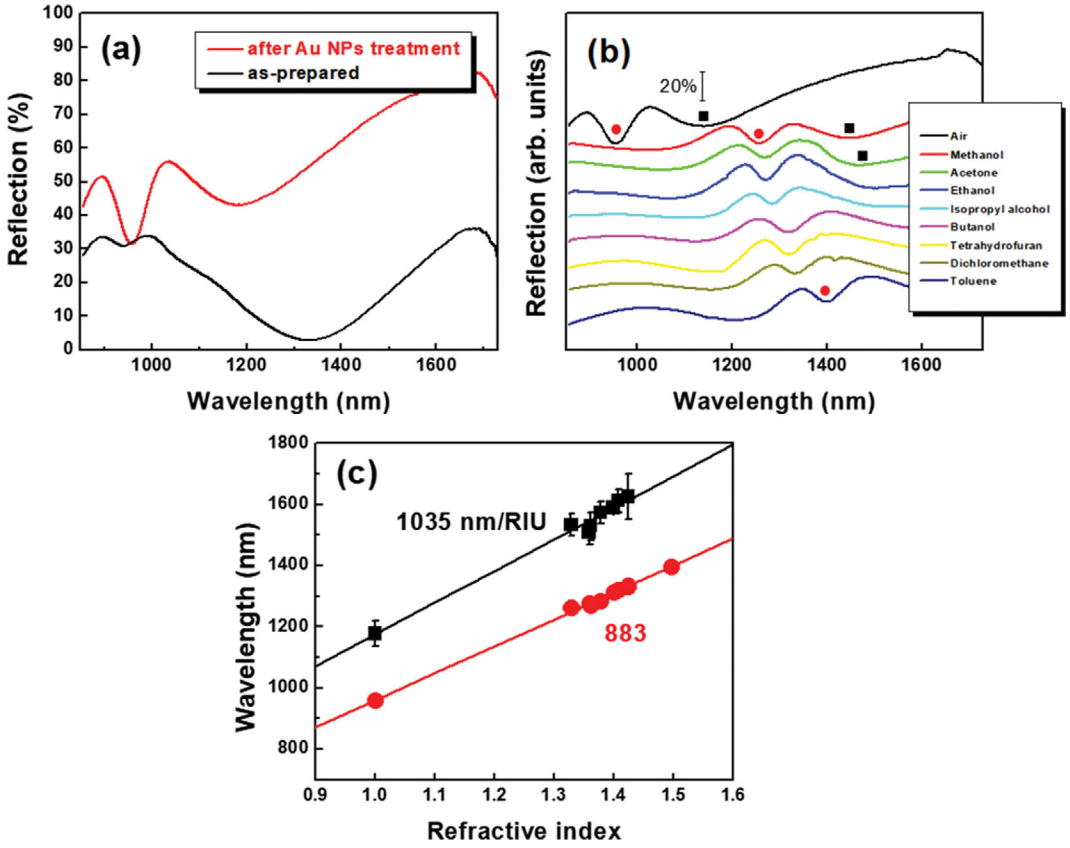

Fig. 6. (a) Experimentally measured normal-incidence optical reflection spectra of AuFON before and after treatment with colloidal Au nanoparticles. (b) SPR sensing tests and (c) SPR dip position versus refractive indices after treatment with colloidal Au nanoparticles.

dip intensity (~22%) can provide an advantage as well as apparent observation in the resonance spectra. Usually, the number of neighboring plasmonic particles increases, and resonance to higher wavelength positions is observed in plasmon hybridization (PH) [30, 57,58]. This hybridization originates from ω_- modes of dipolar oscillation in neighboring particles and is expressed by the decrease in the energy level (eV), frequency of charge oscillation (ω (eV)), and wavelength (nm). Also, it is known that the frequency of charge oscillation (ω_+, ω_-) is proportional to $(R_1/R_2)^{3/2}$ [57,58]. Here, R_1 is the radius of the core particle, and R_2 is the coating thickness in a core-shell sphere particle. It reveals that modulations in the frequency are affected by the geometry of the core-shell spherical particles. Instantly, the SPR dip position gradually shifts with the increase in core diameter and the decrease in coating thickness [59,60]. As a result, the location and intensity of plasmon absorption can be controlled using a thin metal shell of plasmonic particles or a thick dielectric core. Therefore, the shift of the SPR dip position of the dipole mode to a lower wavelength in Fig. 6(a) is predicted to increase the Au coating thickness by treatment with colloidal Au nanoparticles.

For FDTD simulation, several simulations have been attempted with possible structural models, including sphere/hemisphere coating, coating thickness, triangle (or tetrahedron/pyramid) structure between silica microsphere particles, filled interstitial space, bridge structure between neighboring Au-covered silica microsphere particles, and composite structure among them. Although not all results are shown in this report, the interconnected plasmonic particle structure formed by the Au-bridge shows the closest results with experimental reflection spectra regarding both SPR dip position and highly intense Fano absorption. Fig. 7(a) shows a structural illustration using Lumerical FDTD solution software. This interconnected structure between neighboring plasmonic particles was established on a glass substrate with a hemisphere-coated Au layer on silica microsphere particles (1,000 nm in diameter). The simulated reflection spectrum (Fig. 7(b)) shows several reflection dips at 1,296, 947, 647 nm, and other wavelengths. In addition, the intensity (~65%) of the Fano absorption was higher than that (~21%) of the dipole. In particular, the second-order reflection dip observed at 947 nm had a high intensity of 65% and showed an asymmetric, narrow, and deep waveform. The refractive index of the background was set to 1.00, 1.05, 1.10, and 1.15 gradually using FDTD simulation, the sensing test was performed, and the obtained sensitivity was 938 nm/RIU in Fig. 7(c), (d). This value is like the 883 nm/RIU of the Fano absorption obtained experimentally. The treatment of AuFON by colloidal Au nanoparticles focused on improving sensor performance, such as plasmon absorption intensity and sensing sensitivity. A peel-off test was also performed to check the possible enhancement of physical durability, but no improvement was observed, probably because the binding between the silica and the glass substrate was not achieved. Based on the above consideration, it can be predicted that more accurate SPR sensing is possible as the Fano intensity increases.

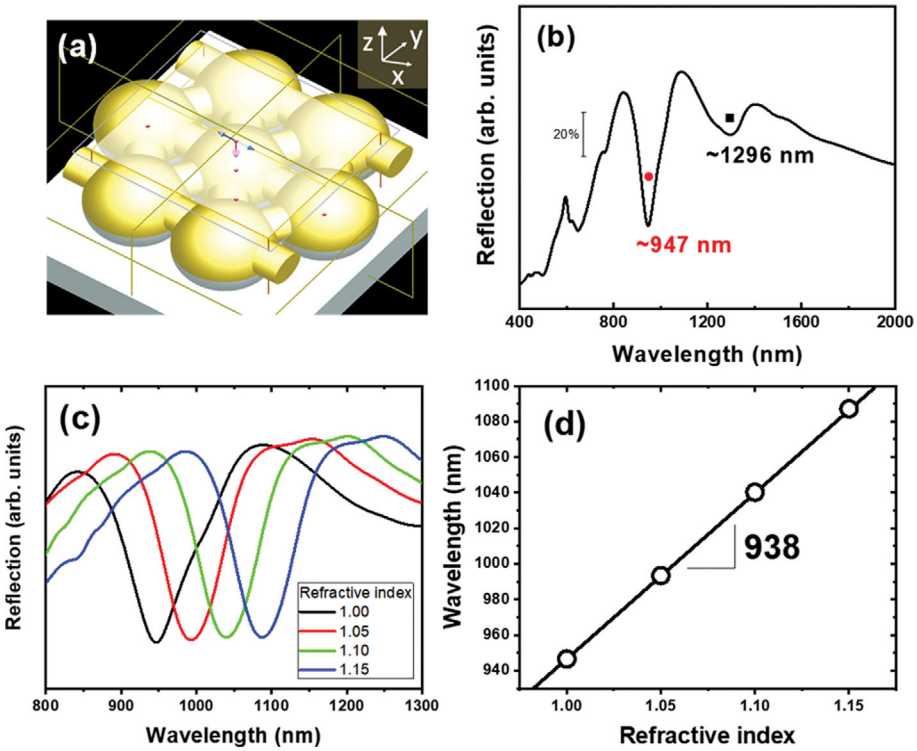

Fig. 7. FDTD simulation. (a) Structural illustration established at the Lumerical FDTD solution, (b) normal-incidence reflection spectrum with a refractive index of 1.00, (c) sensing tests, and (d) SPR dip position versus the refractive index.

CONCLUSIONS

A simple and effective method to enhance the physical durability of the as-prepared AuFON and the strength of the Fano absorption was studied. First, when silica was formed by TMOS treatment in addition to the as-prepared AuFON, excellent physical durability and high sensing sensitivity were observed without any delamination or structural deformation. Second, when the hemisphere-coated Au layers were bound to each other by treatment with colloidal Au nanoparticles, the intensity of the Fano absorption was significantly improved from 3-5 to 22%. Also, the FDTD simulation exhibited the same trend as the experimental results.

ACKNOWLEDGEMENTS

This research was supported by the Korea Electric Power Corporation (R22EA08) and Korea Institute of Energy Technology Evaluation and Planning (20192810100007A).

REFERENCES

1. J. Homola, *Anal. Bioanal. Chem.*, **377**, 528 (2003).
2. J. Homola, *Chem. Rev.*, **108**, 462 (2008).
3. G.-Y. Lee, M. Kim, Y.-J. Quan, M.-S. Kim, T. J. Y. Kim, H.-S. Yoon, S. Min, D.-H. Kim, J.-W. Mun, J. W. Oh, I. G. Choi, C.-S. Kim, W.-S. Chu, J. Yang, B. Bhandari, C.-M. Lee, J.-B. Ihn and S.-H. Ahn, *J. Mech. Sci. Technol.*, **32**, 987 (2018).
4. B. B. Choi, J. H. Jo, J. Bice, C. Taylor, P. Jiang and S. J. Yoo, *Int. J. Energy Res.*, **45**, 19535 (2021).
5. X. Bévenot, A. Trouillet, C. Veillas, H. Gagnaire and M. Clément, *Meas. Sci. Technol.*, **13**, 118 (2001).
6. A. Hosoki, M. Nishiyama, H. Igawa, A. Seki, Y. Choi and K. Watanabe, *Sens. Actuators B Chem.*, **185**, 53 (2013).
7. C. Fang, L. Shao, Y. Zhao, J. Wang and H. Wu, *Adv. Mater.*, **24**, 94 (2012).
8. H. K. Yip, X. Zhu, X. Zhuo, R. Jiang, Z. Yang and J. Wang, *Adv. Opt. Mater.*, **5**, 1700740 (2017).
9. Z. Fang and X. Zhu, *Adv. Mater.*, **25**, 3840 (2013).
10. E. M. Larsson, C. Langhammer, I. Zorić and B. Kasemo, *Science*, **326**, 1091 (2009).
11. Y. Fang, B. M. Phillips, K. Askar, B. Choi, P. Jiang and B. Jiang, *J. Mater. Chem. C*, **1**, 6031 (2013).
12. T. K. Sau, A. L. Rogach, F. Jäckel, T. A. Klar and J. Feldmann, *Adv. Mater.*, **22**, 1805 (2010).
13. Y. Sun and Y. Xia, *Anal. Chem.*, **74**, 5297 (2002).
14. B. Choi, X. Dou, Y. Fang, B. M. Phillips and P. Jiang, *Phys. Chem. Chem. Phys.*, **18**, 26078 (2016).
15. B. B. Choi, B. Kim, Y. Chen and P. Jiang, *J. Electrochem. Sci. Technol.*, **12**, 167 (2021).
16. O. A. Hazzazi, G. A. Attard, P. B. Wells, F. J. Vidal-Iglesias and M. Casadesus, *J. Electroanal. Chem.*, **625**, 123 (2009).
17. B. B. Choi, B. Kim, J. Bice, C. Taylor and P. Jiang, *J. Ind. Eng. Chem.*, **116**, 321 (2022).
18. D. Mortazavi, A. Z. Kouzani and K. C. Vernon, *Prog. Electromagn. Res.*, **130**, 429 (2012).
19. J. A. Fan, C. Wu, K. Bao, J. Bao, R. Bardhan, N. J. Halas, V. N. Mano-

haran, P. Nordlander, G. Shvets and F. Capasso, *Science*, **328**, 1135 (2010).
20. Y. Xia and N. J. Halas, *MRS Bull.*, **30**, 338 (2005).
21. K. M. Mayer and J. H. Hafner, *Chem. Rev.*, **111**, 3828 (2011).
22. K. Askar, B. M. Phillips, Y. Fang, B. Choi, N. Gozubenli, P. Jiang and B. Jiang, *Colloids Surf. A Physicochem. Eng. Asp.*, **439**, 84 (2013).
23. Y.-J. Lee, N. B. Schade, L. Sun, J. A. Fan, D. Ri Bae, M. M. Mariscal, G. Lee, F. Capasso, S. Sacanna, V. N. Manoharan and G.-R. Yi, *ACS Nano*, **7**, 11064 (2013).
24. Y. Chen and H. Ming, *Photonic Sensors*, **2**, 37 (2012).
25. B. M. Phillips, P. Jiang and B. Jiang, *Appl. Phys. Lett.*, **99**, 191103 (2011).
26. Y. Shen, J. Zhou, T. Liu, Y. Tao, R. Jiang, M. Liu, G. Xiao, J. Zhu, Z. K. Zhou, X. Wang, C. Jin and J. Wang, *Nat. Commun.*, **4**, 1 (2013).
27. Z. Liu, M. Yu, S. Huang, X. Liu, Y. Wang, M. Liu, P. Pan and G. Liu, *J. Mater. Chem. C*, **3**, 4222 (2015).
28. E. M. Hicks, X. Zhang, S. Zou, O. Lyandres, K. G. Spears, G. C. Schatz and R. P. Van Duyne, *J. Phys. Chem. B*, **109**, 22351 (2005).
29. B. B. Choi, B. Kim, Y. Chen, S. J. Yoo, Y. Cho and P. Jiang, *J. Ind. Eng. Chem.*, **99**, 179 (2021).
30. E. Prodan, C. Radloff, N. J. Halas and P. Nordlander, *Science*, **302**, 419 (2003).
31. P. Nordlander, C. Oubre, E. Prodan, K. Li and M. I. Stockman, *Nano Lett.*, **4**, 899 (2004).
32. X. Zhang, S. Ye, X. Zhang and L. Wu, *J. Mater. Chem. C*, **3**, 2282 (2015).
33. C. H. Sun, A. Gonzalez, N. C. Linn, P. Jiang and B. Jiang, *Appl. Phys. Lett.*, **92**, 051107 (2008).
34. X. Zhang, M. A. Young, O. Lyandres and R. P. Van Duyne, *J. Am. Chem. Soc.*, **127**, 4484 (2005).
35. X. Zhu, F. Xie, L. Shi, X. Liu, N. A. Mortensen, S. Xiao, J. Zi and W. Choy, *Opt. Lett.*, **37**, 2037 (2012).
36. Y. Oh, S. Park, M. Kang, J. Choi, Y. Nam and K. Jeong, *Small*, **7**, 184 (2011).
37. B. C. Heo, S. Kim, S. G. Jang, S. Y. Lee and S. Yang, *Adv. Mater.*, **21**, 1726 (2009).
38. M. R. Gonçalves, *J. Phys. D. Appl. Phys.*, **47**, 213001 (2014).
39. N. Verellen, P. Van Dorpe, C. Huang, K. Lodewijks, G. A. E. Vandenbosch, L. Lagae and V. V. Moshchalkov, *Nano Lett.*, **11**, 391 (2011).
40. J. Sun, G. Li and W. Z. Liang, *Phys. Chem. Chem. Phys.*, **17**, 16835 (2015).
41. B. Luk'Yanchuk, N. I. Zheludev, S. A. Maier, N. J. Halas, P. Nordlander, H. Giessen and C. T. Chong, *Nat. Mater.*, **9**, 707 (2010).
42. W.-S. Chang, J. B. Lassiter, P. Swanglap, H. Sobhani, S. Khatua, P. Nordlander, N. J. Halas and S. Link, *Nano Lett.*, **12**, 4977 (2012).
43. J. B. Lassiter, H. Sobhani, M. W. Knight, W. S. Mielczarek, P. Nordlander and N. J. Halas, *Nano Lett.*, **12**, 1058 (2012).
44. T. Feng, J. Xiang, C. Liu and Z. Geng, *Opt. Commun.*, **530**, 129172 (2023).
45. D. M. Welakuh and P. Narang, *ACS Photonics*, **9**, 2946 (2022).
46. M. M. Petrić, M. Kremser, M. Barbone, A. Nolinder, A. Lyamkina, A. V. Stier, M. Kaniber, K. Müller and J. J. Finley, *Nano Lett.*, **22**, 561 (2022).
47. G. S. Attard, J. M. Corker, C. G. Göltner, S. Henke and R. H. Templer, *Angew. Chem. Int. Ed. English*, **36**, 1315 (1997).
48. K. M. Kulinowski, P. Jiang, H. Vaswani and V. L. Colvin, *Adv. Mater.*, **12**, 833 (2000).
49. P. Jiang, J. Cizeron, J. F. Bertone and V. L. Colvin, *J. Am. Chem. Soc.*, **121**, 7957 (1999).
50. O.-H. Kim, Y.-H. Cho, S. H. Kang, H.-Y. Park, M. Kim, J. W. Lim, D. Y. Chung, M. J. Lee, H. Choe and Y.-E. Sung, *Nat. Commun.*, **4**, 2473 (2013).
51. X. Zhou, X. Cheng, Y. Zhu, A. A. Elzatahry, A. Alghamdi, Y. Deng and D. Zhao, *Chin. Chem. Lett.*, **29**, 405 (2018).
52. S. Li, M. Zhang and H. Wang, *Sci. Rep.*, **11**, 17158 (2021).
53. H. Baur, K. Lempenauer, M. Hartweg, G. Stephani, O. Andersen and O. Delverdier, in *Materials for transportation technology*, John Wiley & Sons, Ltd, 95 (2000).
54. P. Jiang, J. F. Bertone and V. L. Colvin, *Science*, **291**, 453 (2001).
55. S. Coyle, M. C. Netti, J. J. Baumberg, M. A. Ghanem, P. R. Birkin, P. N. Bartlett and D. M. Whittaker, *Phys. Rev. Lett.*, **87**, 15 (2001).
56. M. Brust, M. Walker, D. Bethell, D. J. Schiffrin and R. Whyman, *J. Chem. Soc. Chem. Commun.*, **7**, 801 (1994).
57. C. Radloff and N. J. Halas, *Nano Lett.*, **4**, 1323 (2004).
58. N. J. Halas, S. Lal, S. Link, W. Chang, D. Natelson, J. H. Hafner and P. Nordlander, *Adv. Mater.*, **24**, 4842 (2012).
59. Q. Li, C. W. Kuo, Z. Yang, P. Chen and K. C. Chou, *Phys. Chem. Chem. Phys.*, **11**, 3436 (2009).
60. E. Prodan, P. Nordlander and N. J. Halas, *Nano Lett.*, **3**, 1411 (2003).